Future Journal of Pharmaceutical Sciences

RESEARCH

Open Access

Optimization of *Lagunaria patersonii* leaf extract employing Box–Behnken design and dual-wavelength approach of tiliroside linked to anti-inflammatory activity

Mayar M. Eladl[1*], Ahmed A. El-Ashmawy[2], Mahmoud T. Abo-Elfadl[3,4], Nabaweya M. El-Fiky[1], Nabil M. Selim[1] and Amira K. Elmotayam[1]

Abstract

Background *Lagunaria patersonii*, a valuable member of the Malvaceae family, holds growing economic and therapeutic interest. This study aimed to optimize the ethanolic extraction of its leaves to maximize both extract yield and concentration of tiliroside, a bioactive compound with known antioxidant and anti-inflammatory properties. Optimization was performed using Box–Behnken Design (BBD) evaluating three variables: plant material/solvent ratio, ethanol/water ratio, and extraction time. Tiliroside concentration was optimized using a dual-wavelength absorbance method which validated by UPLC-ESI–MS.

Results Increasing the plant material/solvent ratio (Factor A) significantly increased the yield by 26-fold compared to extraction time (Factor C), while a higher ethanol/water ratio (Factor B) significantly reduced the yield. Biologically, the optimized extract demonstrated strong antioxidant activity estimated by reactive oxygen species inhibition. Importantly, the isolated tiliroside significantly inhibited nitric oxide, tumor necrosis factor-α and interleukin-6 more than the optimized extract. The BBD approach provided key insights, enabling the optimization of the extract.

Conclusion The study effectively optimized the extraction of *L. patersonii* leaves and highlighted the valuable antioxidant and anti-inflammatory properties of both the optimized extract and its major compound, tiliroside. The integrated use of BBD and dual-wavelength tracking demonstrated significant value in enhancing both yield and bioactivity, offering a promising platform for developing plant-based anti-inflammatory agents. The approach applied was proved to be cost-effective.

Keywords *Lagunaria patersonii*, Malvaceae, Tiliroside, Response surface methodology, Box–Behnken design

*Correspondence:
Mayar M. Eladl
mayar.eladl@pharma.cu.edu.eg
Full list of author information is available at the end of the article

Springer Open

© The Author(s) 2025. **Open Access** This article is licensed under a Creative Commons Attribution 4.0 International License, which permits use, sharing, adaptation, distribution and reproduction in any medium or format, as long as you give appropriate credit to the original author(s) and the source, provide a link to the Creative Commons licence, and indicate if changes were made. The images or other third party material in this article are included in the article's Creative Commons licence, unless indicated otherwise in a credit line to the material. If material is not included in the article's Creative Commons licence and your intended use is not permitted by statutory regulation or exceeds the permitted use, you will need to obtain permission directly from the copyright holder. To view a copy of this licence, visit http://creativecommons.org/licenses/by/4.0/.

Background

Malvaceae plants are widely recognized as important icons of the tropics and subtropics, with a prominent economic and therapeutic reputation. It includes 244 genera and more than 4225 species of trees, shrubs, and herbs [1–3]. Genus *Lagunaria* comprises two species: *L. patersonii* (Andrews) G. Don. and *L. queenslandica* Carven. Cow-itch; *L. patersonii* is the only species cultivated in Egypt. It was used as a source of fiber that is used for fishing lines, nets, and ropes. Few reports were found concerning the phytochemical constituents of *L. patersonii* (Andrews) G. Don. Fruits and seeds were reported to contain polyphenols, flavonoids, oleic acid, palmitic acid, as well as cyclopropene fatty acids like malvalic acid, sterculic acid, and trace quantities of dihydrosterculic acid. Concerning the biological activity of *L. patersonii* (Andrews) G. Don., the aqueous fraction obtained from the fruits and seeds residue was reported to have antioxidant activity measured by DPPH inhibition [4]. The alcoholic and petroleum ether extracts of the plant were reported to have promising insecticidal activity against *Drosophila melanogaster* (Meig), also known as laboratory flies, *Tribolium confusum* (DUV), commonly known as confused flour beetles, and cotton leafworms (*Spodoptera littoralis* (Boisd) [5].

Extraction of secondary metabolites was affected by several parameters such as plant material/solvent ratio, solvents, and time. Their variation is reflected in their yield. The effect of the aforementioned factors on the extraction procedure was reported on some plants of the family Malvaceae: *Hibiscus rosa-sinensis* L., *Abutilon indicum* L., *Gossypium herbaceum* L., and *Hibiscus mutabilis* L. [6, 7], but nothing was traced concerning *L. patersonii*. Therefore, it is important to choose the appropriate method to prepare the optimized extract containing the biologically active constituents.

The application of a wavelength-absorbance approach for maximizing amount of tiliroside in *Lagunaria patersonii* was critical due to the compound's dual λ_{max} behavior, which reflects its extended conjugated chromophore and multifunctional aromatic substituents. Utilizing this dual-wavelength method ensures improved selectivity and precision, particularly when overlapping signals could compromise single λ_{max} detection. Validation using UPLC-ESI–MS further confirmed the reliability of this strategy, strengthening its utility in accurately monitoring tiliroside concentration throughout the extraction process. Importantly, this analytical approach can be extended to other polyphenolic compounds such as kaempferol derivatives, rutin, or chlorogenic acid, which often exhibit similar dual absorption due to $\pi \rightarrow \pi^*$ and $n \rightarrow \pi^*$ electronic transitions. Adopting a dual λ_{max} strategy not only enhances detection sensitivity for structurally complex metabolites but also enables more robust correlation with biological activity, supporting more rational optimization of extract formulations in pharmacological and nutraceutical research.

Tiliroside "kaempferol–3-*O*-*β*-D-(6′′-*O*-*p*-coumaroyl)-glucopyranoside" is a flavonoid glycoside, an important secondary metabolite that is crucial to the chemotaxonomy of the family Malvaceae and has been identified as the most common compound among its members [8, 9]. It has two maximum absorbance wavelengths (λ max) at 265 nm and 346 nm [10]. It is well known that some compounds were reported to have a constant ratio of absorbance at certain wavelengths, known as an isosbestic [11]. The concentration of a solution and its absorbance are known to be linearly related, as stated by the Beer–Lambert law [12, 13]. When a compound, such as tiliroside, exhibits two wavelengths of maximum absorbance, each of these wavelengths will correlate with the corresponding concentrations through linear regression constants. As a result, the absorbance ratio between the two wavelengths remains constant across different concentrations of the compound.

The design of experiments (DOE) is a focused approach employed to investigate the significance of different variables influencing a particular process, the relationships among these factors, and their effects on the outcomes of the process. The main benefit of DOE lies in recognizing interactions between variables and finding the optimal response within the design framework. This is achieved by reducing the number of experiments, which conserves time, effort, and resources and interprets results more straightforwardly [14]. The response surface methodology (RSM) is a robust analytical tool that employs DOE to conjecture the conditions for optimal response. As a result, the RSM-driven optimization process is instant and eliminates the need for further experiments or simulations [14–17].

BBD is commonly used in RSM for optimizing the extraction of biologically active compounds in fields such as bioprocessing, pharmaceuticals, and food engineering [14, 17–20]. It is a fractional-factorial design at three levels, characterized by its second-order structure, and is either rotatable or so [20]. It offers numerous advantages, such as incorporating blocks, not requiring model fit detection, enabling the creation of sequential designs, and allowing for the estimation of quadratic model parameters. The main benefit compared to other designs is that it avoids conducting experiments in extreme conditions, like using the lowest or highest levels of all variables at once, which may be costly or impractical to evaluate [21].

Inflammation is considered a set of evolutionary host responses primarily developed due to external triggers such as injuries, chemicals, radiation, and infections. Currently, excessive research reports that overproduction of high ROS, such as hydrogen peroxide and superoxide anions, induces oxidative damage at the cellular level [22]. Cyclooxygenase 2 (COX-2) and NO are potential biomarkers in the inflammatory process. Specifically, NO plays a key role in the pathophysiology of inflammation. Activated macrophages are thought to be caused by the continuous high production of NO [23]. Macrophages are also involved in the release of pro-inflammatory cytokines like TNF-α and IL-6 in response to inflammatory stimulation. Currently, non-steroidal anti-inflammatory drugs (NSAIDs) are the classically used drugs worldwide for treating both acute and chronic inflammatory pain. Despite their efficacy, they lead to serious side effects [24]. Therefore, there is an increasing need to find natural anti-inflammatory drugs with fewer side effects. Plants belonging to the family Malvaceae were reported to have anti-inflammatory activities in various in vitro assays [25]. This study aimed to increase the yield of the extract of *L. patersonii* leaves and maximize the amount of tiliroside in the yield using response surface methodology (RSM) and employing BBD, as well as investigating the antioxidant and anti-inflammatory properties of the optimized extract and tiliroside. It is worth mentioning that one of the primary goals was to establish a green extraction method by reducing the volume of the extraction solvent.

Material and methods

Chemicals, kits, and cell lines

The solvents utilized in this study, ethanol and methanol, were of analytical grade and supplied from PioChem laboratory chemicals, Cairo, Egypt. Tiliroside analytical standard (Sigma-Aldrich, Germany), Dexamethasone analytical standard (Merck, Darmstadt, Germany), LC/MS-grade solvents formic acid, and acetonitrile (Sigma-Aldrich, Germany). ROS fluorometric assay kit (Green), Catalog Number: E-BC-K138-F, from Elabscience, Wuhan, China, lipopolysaccharides (LPS) from *Escherichia coli* O55:B5 (Merck, Darmstadt, Germany). Colorimetric assay kit (nitrate reductase method), Cat Number: E-BC-K135-M kit (Elabscience, Wuhan, China), Quantikine enzyme-linked immunosorbent assay (ELISA). Human TNF-α immunoassay kit, IL-6 ELISA Kit (colorimetric), NBP1-92697 (Novus Biologicals, Colorado, USA), and murine RAW 264.7 cells were sourced from the American Type Culture Collection (Manassas, VA, USA). They were cultured at 37 °C in Dulbecco's modified Eagle medium (DMEM), supplemented with 10% fetal bovine serum and 1% penicillin sulfate, in a humidified atmosphere containing 5% CO_2. The cells were stimulated with one µg/ml LPS for 6 h and then treated with different extracts, left with the LPS as positive control, or left without LPS as a negative control.

Preparation of a standard solution of tiliroside

A stock solution of tiliroside was prepared in a glass-stoppered volumetric flask with methanol. The stock solution was serially diluted to achieve selected concentrations, and the absorbance ratio was calculated. The value of the absorbance ratio at each concentration was found to be 0.747 ± 0.014 (mean ± SD, Table S1). So, the absorbance ratio between the two wavelengths remained constant across different concentrations of tiliroside. Hence, we followed 0.747 (the constant value of the absorbance ratio 265/346 is a characteristic feature of tiliroside) to increase the amount of tiliroside in the extract yield.

Optimization of the plant extraction method

The optimization study employed BBD with three factors at three levels, using Design-Expert V.8. It investigated three independent variables (factors) and two dependent variables (responses). Table 1 displays the actual and coded levels. The measured responses **(Y1 & Y2)** and the BBD are shown in Table 2, including a total of seventeen runs, with five center points. The factors and their levels were chosen depending on earlier work [5, 7, 26–29]. The experiments were conducted at room temperature (25 °C) to avoid any degradation of active components, specifically phenolic acids, and flavonoids. The "ethanol/water ratio" was adjusted (95%, 72.5%, and 50%) to study the effects of various polar solvent mixtures.

Table 1 The actual and coded levels of the variables examined in the Box–Behnken design (BBD)

Levels used			
Independent variables	**Low (− 1)**	**Middle (0)**	**High (1)**
Factors (independent variables)			
A: material/solvent ratio	1:5	1:10	1:20
B: ethanol/water ratio%	50	72.5	95
C: extraction time	24 h	48 h	72 h
Response (dependent variables)			
Y1: Yield (g)			
Y2:(265/346 absorbance ratio at an extract concentration of 140 µg/ml)			

Table 2 The Box–Behnken response surface design, along with the associated response values

Std. order	Run #	A: material/solvent ratio %	B: ethanol/water ratio%	C: extraction time (hr.)	Y1 (Yield "g")	Y2 (265/346 absorbance ratio at an extract concentration of 140 µg/ml)
12	1	25/250	95%	72	2.0911	0.543
9	2	25/250	50%	24	3.1467	0.729
16	3	25/250	72.50%	48	2.7012	0.607
14	4	25/250	72.50%	48	2.379	0.695
17	5	25/250	72.50%	48	2.4251	0.649
1	6	25/125	50%	48	0.8633	0.705
6	7	25/500	72.50%	24	4.0605	0.653
8	8	25/500	72.50%	72	4.4159	0.663
2	9	25/500	50%	48	4.2378	0.680
7	10	25/125	72.50%	72	1.2458	0.638
10	11	25/250	95%	24	1.9474	0.512
3	12	25/125	95%	48	0.8901	0.525
4	13	25/500	95%	48	1.8767	0.516
5	14	25/125	72.50%	24	1.2176	0.638
15	15	25/250	72.50%	48	2.3434	0.593
11	16	25/250	50%	72	3.0166	0.641
13	17	25/250	72.50%	24	2.431	0.662

A: material/solvent ratio %; B: ethanol/water ratio%, C: extraction time (hr.); Y1: yield g

Y2: (265/346 absorbance ratio at an extract concentration of 140 µg/ml)

Preparation of extract

Leaf powder (25 g per run) was subjected to maceration at ambient temperature, utilizing various ethanol/water ratios, different material-to-solvent ratios, and varying extraction durations as outlined in Tables 1 and 2 of the optimization study. The extracts were then evaporated using a Buchi RR-300 rotary evaporator (USA) at 45 °C to give a green residue. The yield (Y1) of each run was weighed, and the ratio of absorbance at wavelengths λ max 265 and 346 nm (265/346 absorbance ratio) (Y2) at the extract concentration of 140 µg/ml (selected concentration) is illustrated in Table 2. A concentration of 140 µg/mL was selected for comparative absorbance analysis across all Box–Behnken runs, as it was consistently present in the validated calibration curves for each run. This allowed for standardized wavelength-ratio measurements and minimized variability due to interpolation.

Preparation of a stock solution for the plant extract

A stock solution was prepared by dissolving 0.05 g of dried residue in 50 mL of methanol, resulting in a concentration of 1000 µg/ml. This solution was then serially diluted with a methanol–water mixture 50:50 (v/v) to achieve the desired concentration. The absorbance of the prepared solutions was measured spectrophotometrically (Shimadzu Ultraviolet (UV)-1800 Serial No. A116351) at λ max 265 nm and 346 nm against a blank of methanol–water (50:50, v/v) (Y2). Table 2.

Isolation of the major compound from the optimized extract

The optimized extract was subjected to fractionation using different solvents according to their polarity (hexane, methylene chloride, and ethyl acetate). The ethyl acetate fraction was concentrated, and a yellow residue (40 mg) was precipitated, purified through filtration, and repeated washing with methanol, to give needle crystals. It was identified using physical, co-chromatographic TLC technique, alongside with authentic sample and spectroscopic technique.

Antioxidant activity

Estimation of reactive oxygen species (ROS)

"Murine RAW 264.7 cells" were used for ROS detection. 1×10^4 cells were cultured in a black 96-well cell culture plate (Cat. no 33396, SPL, Seoul, South Korea). Three independent wells were aliquoted for each of the negative control, LPS, optimized extract, and tiliroside. ROS was measured according to the manufacturer's protocol using reactive fluorescence ROS assay kit (Green), Cat Number: E-BC-K138-F from Elabscience, Wuhan, China. [30, 31] at excitation/emission 502/520 nm.

Anti-inflammatory activity

The RAW 264.7 murine macrophage cell line was maintained in a 6-well culture plate at a density of 1×10^6 cells/ 2 ml medium and sensitized with 1 µg/ml of LPS, except one well as a negative control. After 6 h, both optimized extract and tiliroside were applied and adjusted to a final concentration of 50 µg/ml. Dexamethasone (Merck, Darmstadt, Germany) was used as a positive control at a concentration of 100 nm. Therefore, the five wells contained two different extracts (optimized and tiliroside), dexamethasone and LPS alone, as well as negative control cells. After 48 h of incubation, the supernatant and the cell pellets were collected from each well for further anti-inflammatory quantification [32]. Supernatant samples were used for detecting NO, TNF-α, and IL-6.

Dose–response curves of ROS, NO, TNF-α, and IL-6

The RAW 264.7 cells were cultured in 96-well cell culture plates at a density of 10^4 cells/ well. After settling down, the cells were sensitized by LPS as before and then treated with both tiliroside and optimized extract at concentrations of 75, 50, 25, and 12.5 µg/mL. The dexamethasone was used as positive control at concentrations of 150, 100, 50, and 25 nM. Negative control cells were left untreated to measure the baseline of each inflammatory mediator. LPS-treated cells were left as a control for the inflammatory response of each mediator. The IC_{50} values of both the tiliroside and the optimized were plotted for each mediator (Table 8).

NFkB protein expression

The murine macrophage cells, RAW 264.7 cell line, was cultured on 8-well cell culture slides (SPL, Seoul, South Korea) at a density of 10^4 cells / 250 µL/ well. The cells were sensitized by LPS as above and then treated with the samples, tiliroside and optimized, and adjusted to obtain final concentrations equal to 50 µg/mL, respectively. The experiment was performed for 24 h. of incubation. After that, the cells were fixed with 4% paraformaldehyde and permeabilized with 0.1% Triton X-100. The cells were then blocked with 1% bovine serum albumin and incubated overnight at 4 °C with the rabbit polyclonal anti-NFkB p65 antibody, ab16502 (Abcam, Cambridge, UK) at dilution of 1:200. After extensive washing, the cells were incubated with the secondary antibody goat anti-rabbit IgG (Alexa Fluor®488) ab150077 (Abcam, Cambridge, UK) at 1/250 dilution. After washing and air drying, the glycerol mounting medium with DAPI (ab188804, Abcam, Cambridge, UK) was used as an anti-fade and as a counterstain for the nucleus. The cells were then visualized under the fluorescent microscope AxioImager Z2 (Zeiss, Jena, Germany), and the intensity of the fluorescence was measured using Zen11 Blue edition software (Zeiss, Jena, Germany).

Statistics

The statistical evaluation of the BBD was performed using Design-Expert software (version 8). The bioassay data were analyzed with Statistical Package for Social Sciences (SPSS) software (version 22). A one-way analysis of variance (ANOVA) and Tukey's multiple comparison test were employed at a 95% confidence level to assess significance. The findings are expressed as mean ± SD.

UPLC-ESI–MS analysis

Mass spectrometric analysis (UPLC-ESI–MS) was conducted on selected runs 2 and 11, as well as the optimized extract (Waters Corp., Milford, MA, USA). The column used was an ACQUITY UPLC—BEH C18, 1.7 µm—2.1×50 mm. The solvent system comprised (A) water with 0.1% formic acid and (B) acetonitrile with 0.1% formic acid. The flow rate was set at 200 µl/min. The B ratio began at 10% for 2 min and then increased to 30%, 70%, 90%, and 100% over 3 min, 10 min, 10 min, and 4 min, respectively, before returning to a 10% gradient for 3 min. The negative mode MS scan was performed under the following conditions: capillary voltage of 3 kV, cone voltage of 30 V, and source temperature of 440 °C. Nitrogen was used as the mobile phase at a flow rate of 900.

Spectroscopic analysis

Using a Bruker NMR-spectrometer (Karlsruhe, Germany), **^{1}H-NMR** (400 MHz) and **^{13}C** (100 MHz) spectra were recorded in appropriate deuterated chloroform (CDCl3). Tetramethyl silane (TMS) was used as the internal standard, chemical shift values were expressed in δ ppm, and the coupling constants were expressed in Hz.

Electrospray Ionization Mass Spectrometry (ESI–MS): UPLC MS/MS "Waters" 3100 (USA) instrument was used, Detector, TQ Detector (ACQUITY ultra performance LC).

Results

Box–Behnken design (BBD)

Experimental design and model validation

Table 2 displays the BBD used for optimizing the extraction of *L. patersonii*. The BBD matrix outlines each experimental run-in individual rows, along with their respective responses [Yield (Y1) and the ratio of absorbance at λ max 265 and 346 nm at 140 µg/ml extract concentration (265/346 absorbance ratio) (Y2)]. Table 3 presents the model summaries, "lack-of-fit tests", and "sequential sums of squares" for each response,

Table 3 Sequential model fitting for the yield (Y1) and the 265/346 absorbance ratio at an extract concentration of 140 µg/ml (Y2)

Yield (Y1)							**265/346 absorbance ratio at an extract concentration of 140 µg/ml (Y2)**					
Source	**Sum of squares**	**Mean square**	**DF**	**F-value**	***P*-value**	**Remarks**	**Sum of squares**	**Mean square**	**DF**	**F-value**	***P*-value**	**Remarks**
Sequential sum of squares												
Mean	100.28	100.28	1				6.67	6.67	1			
Linear	15.96	5.32	3	21.57	< 0.0001		0.055	0.018	3	13.24	0.0003	Suggested
2FI	1.47	0.49	3	2.83	0.0929		3.619E − 003	1.206E − 003	3	0.85	0.4990	
Quadratic	1.29	0.43	3	6.78	0.0177	Suggested	6.116E − 003	2.039E − 003	3	1.76	0.2426	
Cubic	0.36	0.12	3	6.04	0.0575	Aliased*	1.317E − 003	4.389E − 004	3	0.26	0.8528	Aliased*
Residual	0.080	0.020	4				6.808E − 003	1.702E − 003	4			
Total	119.45	7.03	17				6.74	0.40	17			
Lack-of-fit tests												
Linear	3.13	0.35	9	17.30	0.0073		0.011	1.228E − 003	9	0.72	0.6868	Suggested
2FI	1.65	0.28	6	13.74	0.0121		7.432E − 003	1.239E − 003	6	0.73	0.6539	
Quadratic	0.36	0.12	3	6.04	0.0575	Suggested	1.317E − 003	4.389E − 004	3	0.26	0.8528	
Cubic	0.000		0			Aliased*	0.000		0			Aliased*
Pure error*	0.080	0.020	4				6.808E − 003	1.702E − 003	4			
	Std. Dev	**R-Squared**	**Adjusted R-Squared**	**Predicted R-Squared**	**PRESS**		**Std. Dev**	**R-Squared**	**Adjusted R-Squared**	**Predicted R-Squared**	**PRESS**	
Model summary statistics source												
Linear	0.50	0.8327	0.7941	0.6540	6.63		0.037	0.7534	0.6965	0.5891	0.030	Suggested
2FI	0.42	0.9095	0.8552	0.5524	8.58		0.038	0.8034	0.6854	0.4275	0.041	
Quadratic	0.25	0.9768	0.9470	0.6898	5.94	Suggested	0.034	0.8878	0.7436	0.5622	0.032	
Cubic	0.14	0.9958	0.9832			Aliased	0.041	0.9060	0.6240		+	Aliased

*Statistically significant: $p < 0.05$

DF: Degree of freedom, F-value: Fisher value, R-Squared: Regression Coefficient, 2FI: 2-factor interaction

*Aliased model: a model where certain effects cannot be independently estimated due to design constraints, * pure error: variability observed in repeated experiments under identical conditions

Table 4 The *p*-values and coefficient estimate for the two analyzed responses

	Y_1: Yield		Y_2: (265/346 absorbance ratio at an extract concentration of 140 µg/mL)	
	***p*-value prob > F**	**Coefficient estimate**	***p*-value prob > F**	**Coefficient Estimate**
Intercept		2.46		0.63
A-material/solvent ratio	< 0.0001	1.30	0.9595	6.783E − 004
B-ethanol/water ratio%	0.0004	− 0.56	< 0.0001	− 0.082
C-time	0.5945	0.050	0.6638	− 5.828E − 003
AB	0.0021	− 0.60		
AC	0.5367	0.082		
BC	0.6036	0.068		
A^2	0.2548	− 0.15		
B^2	0.0288	− 0.34		
C^2	0.0098	0.43		

*Statistically significant at $p < 0.05$

encompassing four models: "quadratic, cubic, 2-factor interaction (2FI), and linear". These evaluations were conducted to assess the adequacy of the models. The model's reliability was assessed using ANOVA to evaluate the impact of each factor on individual responses. For the first response (Y1), a quadratic model was chosen based on: (*i*) a significant *p*-value from the sum-of-squares analysis (*p*-value = 0.0177), (*ii*) a nonsignificant lack of fit (*p*-value = 0.0575), and (*iii*) a maximized adjusted R^2 (0.9470). For the second response (Y2), a linear model was selected due to: (*i*) a significant *p*-value from the sum-of-squares analysis (*p*-value = 0.0003), (*ii*) a nonsignificant lack of fit (*p*-value = 0.6868), and (*iii*) a maximized adjusted R^2 (0.6965).

Verification of model adequacy

The model's accuracy and predictive capability were validated as shown in Fig. S1. For each run, the predicted values of Y1 and Y2 were computed and compared with the experimental results. Figure S1 demonstrates that the actual outcomes closely matched the predicted values, both for the yield (Fig. S1a) and for the ratio (Fig. S1b). This indicates that the model fits well and has strong predictive power, thereby improving the understanding of the relationship between the dependent and independent variables.

The yield (Y1)

The values of the yield (Y1) ranged from 0.8633 to 4.4159 g, as detailed in Table 2. Table 3 provides sequential model fitting data for the yield. The statistical evaluation revealed that the quadratic model was the most suitable, being the only model with a significant *p*-value ($p < 0.0001$) in the sum-of-squares analysis and a nonsignificant lack of fit ($p = 0.0575$, Table 3). Table 4 outlines the coefficient estimates and *p*-values for each model term. The linear coefficients (A, B), two quadratic coefficients (B^2 and C^2), and one interaction coefficient (AB) had a significant impact on the yield ($p < 0.05$, Table 4). The material/solvent ratio (factor A) had the most substantial effect, with a coefficient estimate of + 1.30 and a highly significant *p*-value ($p < 0.0001$). The positive sign indicates a direct relationship, where an increase in the volume of extraction solvent compared to the amount of plant material leads to the greatest increase in yield. On the other hand, the ethanol/water ratio (factor B) with a coefficient estimate of -0.56 had a significant effect on yield ($p = 0.0004$). The negative sign indicates a decreasing effect of the ethanol/water ratio on the yield. Increasing the water content in the ethanol/water solvent mixture led to a higher yield. Conversely, the extraction time (factor C) with a regression coefficient of 0.050 did not significantly affect the yield ($p = 0.5945$). Factor A (material-to-solvent ratio) had a strong increasing effect (+ 1.30), while Factor B (ethanol-to-water ratio %) showed a weaker but decreasing effect (− 0.56). Their interaction yielded a coefficient estimate of − 0.60, indicating that the influence of ethanol-to-water ratio was stronger than that of the material-to-solvent ratio when considered in combination, although the interaction effect remained lower in magnitude compared to Factor A alone. This means that Factor A (material-to-solvent ratio) has the strongest effect. On the other hand, Factor C (Time) by itself was nonsignificant, and therefore, its interactions with other factors (A or B) were also nonsignificant. However, the two quadratic terms (B2 and C2) had significant impacts, with *p*-values of 0.0288 and 0.0098, respectively. The quadratic term for time (C2) had a directly proportional effect on the yield (regression coefficient 0.43), while B2 had a highly significant inversely proportional effect (coefficient estimate = − 0.34). Finally, the interaction term (AB) significantly decreased the yield, with a *p*-value of 0.0021 and a coefficient estimate of − 0.60. The quadratic term (A2) and interaction terms (AC and BC) did not have significant effects, as indicated by their p-values ($p > 0.05$, Table 4). Therefore, simplifying the regression equation by removing the nonsignificant terms resulted in the following reduced equation: -

$$\text{Yield} = +2.46 + 1.30A - 0.56B - 0.60AB - 0.34B^2 + 0.43C^2$$

Figure 1a demonstrates how the material/solvent ratio (A), ethanol/water ratio (B), and their interactions influence the yield, using 3D response surface plots. These plots effectively illustrate the importance of the regression equations by highlighting peaks and troughs. As shown in Fig. 1a, the yield was lowest at both 50% and 95% ethanol/

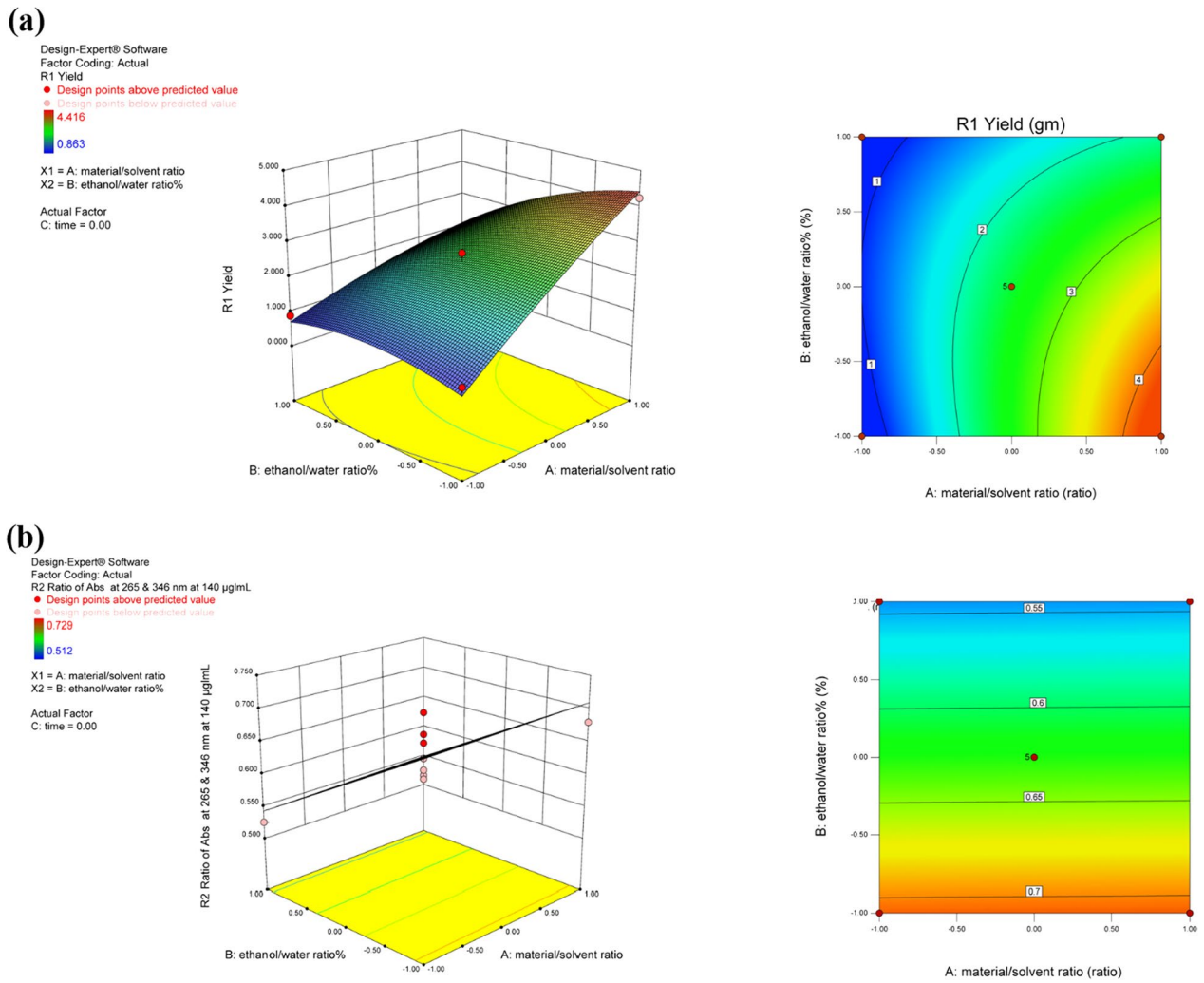


Fig. 1 Three-dimensional response surface plots for **a** yield (Y1): Effect of A (material/solvent ratio), B (ethanol/water ratio% %), and their interaction on the yield. **b** 265/346 absorbance ratio at an extract concentration of 140 µg/ml (Y2): Effect of A (material/solvent ratio), B (ethanol/water ratio), and their interaction on the ratio

water ratios. Moreover, at a low material/solvent ratio of 1:5, the ethanol/water ratio had no impact. Conversely, at a 50% ethanol/water ratio, increasing the material/solvent ratio markedly enhanced the yield.

The 265/346 absorbance ratio at an extract concentration of 140 µg/ml (Y2) is detailed in Table 2 (Table 3), which compiles sequential model fitting data. The ratio ranged from 0.512 to 0.729, as shown in Table 2. The linear model was selected because it was the only model that exhibited both a significant p-value in the sum-of-squares analysis ($p=0.0003$) and a nonsignificant lack of fit ($p=0.6868$), as demonstrated in Table 3. It was determined that the ethanol/water ratio (B) was the only factor with a significant effect on the 265/346 absorbance ratio (Table 4), while the material/solvent ratio (A) and time (C) had no significant impact. Simplifying the regression equation by removing the nonsignificant terms resulted in the following equation:

$$\text{The 265/346 absorbance ratio at an extract concentration of } 140\mu\text{g/ml} = +0.63 - 0.082\text{B}$$

Figure 1b visually illustrates the impact of the material/solvent ratio (A) and its interaction with the ethanol/water ratio (B) on the 265/346 absorbance ratio. The 265/346 absorbance ratio increased when the material/solvent ratio was at a high level (1:20) and the ethanol/water ratio was at a low level (50%).

Figure 2 presents the coefficient estimates for the several factors influencing the two responses (amount of yield and 265/346 absorbance ratio). The material/solvent ratio had a significant increasing impact on the

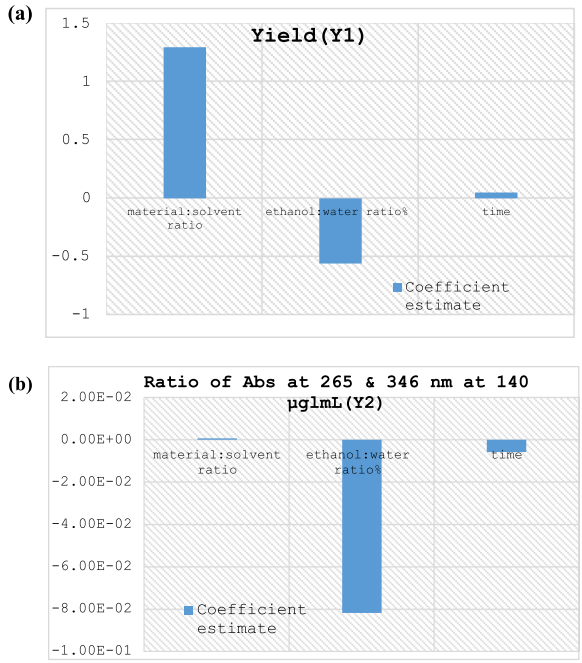


Fig. 2 Coefficient estimates for the factors examined concerning each response. **a** Yield **b** 265/346 asorbance ratio at an extract concentration of 140 µg/ml

amount of the yield, while the ethanol/water ratio had a significant decreasing effect, with the highest magnitude on the amount of the yield (Fig. 2a, Table 4). Figure 2b shows that both material/solvent ratio and time had a decreasing effect, which was nonsignificant on the 265/346 absorbance ratio (Table 4). Noteworthy, the ethanol/water ratio had a significant decreasing effect on the 265/346 absorbance ratio (p-value < 0.05) (Fig. 2b, Table 4).

Model validation

To validate the model, two separate extraction runs (checkpoints) were conducted, which were not part of the design matrix. The model's predicted values closely matched the actual results from these checkpoints (Table 5).

Multiple response optimization.

The run was performed to maximize both yield and the 265/346 absorbance ratio at an extract concentration of 140 µg/ml. To optimize two responses with different targets, a multi-criteria strategy employing numerical optimization through the desirability function was utilized to identify the optimal levels for each extraction run [15, 33]. The numerical optimization feature in Design-Expert depends on the desirability function for the specified factors and responses. This function converts the response variable into a scale from 0 to 1, where a desirability of one indicates the most favorable outcome, and a desirability of zero indicates the least favorable [34]. The numerical optimization aimed to maximize both the yield (Y1) and the 265/346 absorbance ratio at an extract concentration of 140 µg/ml (Y2). The three factors (A, B, and C) were kept within range, achieving a desirability of 0.969 as illustrated in Fig. S2. The highest predicted yield was 4.243 g, obtained using 500 ml of 50% ethanol over 24 h, with a desirability of 0.969.

Table 5 95% confidence interval for the optimized extract (Opt.) and the checkpoints

Optimizations	Goal	Opt	Checkpoint 1	Checkpoint 2
A: Material/solvent ratio		Maximizing both yield and the ratio of absorbance at 265 & 346 nm at 140 µg/ml		
B: Ethanol/water ratio	Lower limit	Yield: 0.863 Ratio: 0.512		
C: Time	Upper limit	Yield: 4.416 Ratio: 0.729		
Y1 (Yield)	95% PI low	3.856	3.649	3.242
	Prediction	4.767	4.418	4.416
	95%PI high	5.678	5.186	4.875
	Observed	4.243	4.657	4.116
Y2 * (265/346 absorbance ratio)	95% PI low	0.619	0.609	0.622
	Prediction	0.715	0.700	0.715
	95%PI high	0.811	0.791	0.808
	Observed	0.747	0.612	0.726
Desirability		0.969		

*The ratio of absorbance at 265 and 346 nm at an extract concentration of 140 µg/ml

The actual yield of the optimized extract, measuring 4.243 g, was within the 95% confidence interval of 3.856–5.678 g. Likewise, the actual 265/346 absorbance ratio for the optimized extract, recorded at 0.747, fell within the 95% confidence interval of 0.619 to 0.811. This validated the response model's adequacy, as it met the anticipated optimization. Thus, the model is both accurate and dependable, illustrating that the BBD can effectively optimize the yield and the 265/346 absorbance ratio at an extract concentration of 140 µg/ml and hence the amount of tiliroside in the yield of *L. patersonii* (Table 5). Consequently, BBD was successfully applied to optimize both the extraction yield and the tiliroside content in *L. patersonii* leaves.

UPLC-ESI–MS analysis

UPLC-ESI–MS was performed to quantify tiliroside to prove the concept of tracking the λ max 265/346 absorbance ratio in the BBD design. It was found that the extracts of run two and run eleven showed the highest and the lowest 265/346 absorbance ratio (0.729 and 0.512), respectively. Therefore, UPLC-ESI–MS evaluated the extracts. The peak area % of tiliroside to total peak areas in the UPLC-ESI–MS chromatograms of run two and run eleven extracts was found to be 8.32% and 0.94%, respectively. Thus, the extract at run two showed the highest concentration of tiliroside and demonstrated the concept of tracking the 265/346 absorbance ratio to increase the amount of tiliroside in the extract. Typically, the two wavelengths were selected (at λ max 265 nm and 346 nm) based on the presence of two maxima of tiliroside at the selected wavelengths. The optimized extract was performed based on maximizing both the yield of the plant and the λ max 265/346 absorbance ratio to maximize the yield of tiliroside. UPLC-ESI–MS was established to confirm the results in Fig. S3. It showed a peak area of 16.44% which is twice the peak area of the highest run (run 2) (Table S2).

Identification of tiliroside

^{1}H NMR (400 MHz, $CDCl_3$) δ_H ppm: 12.57(s,1H,OH-5),7.9 (d, J=8.7 Hz, 2H, H-2′,6′),7.36(d, J=8.7 Hz,2H, H-2′′′,6′′′), 7.3 (d, J=16 Hz, 1H, H-7′′′-β), 6.85(J=8.7 Hz,2H, H-3′, 5′), 6.7 (d, J=8.7 Hz,2H, H-3′′′, 5′′′), 6.2 (d, J=2.0 Hz, 1H, H-8),6.14 (d, J=2.0 Hz,1H,H-6), 6.10 (d, J=15.9 Hz, 1H, H-8′′′ α), 5.1 (d, J=7.5 Hz, 1 H, H′′).

^{13}C NMR (100 MHz, $CDCl_3$) δ_C ppm: 178.05 (C-4), 167.38 (C-9′′′), 164.54 (C-7), 161.58 (C-5), 160.12 (C-4′), 159.78 (C-4′′′), 157.97 (C-2), 157.03 (C-9),145.15 (C-7′′′-β), 133.75 (C-3), 130.80 (C-2′-6′), 129.78 (C-1′),125.69 (C-1′′′), 115.39 (C-3′, 5′),114.64 (C-8′, α), 104.20 (C-10), 98.59 (C- 6), 93.40 (C-8), 76.58 (C-3′′′), 74.40 (C-2′′), 74.31 (C-5′′), 70.32 (C-4′′) 62.87 (C-6′′).

ESI–MS $[M-H]^-$ 593.36, fragments [M-H-*p*-coumaroyl]$^-$ 447, [M-H- *p*-coumaroyl-glucosyl]$^-$ 285. From the following spectral data, ^{1}H NMR, ^{13}C NMR, and ESI–MS data, the compound was identified as tiliroside; known as "Kaempferol-3-*O*-β-D-(6′′-E-*p*-coumaroyl) glucopyranoside" Molecular formula: $C_{30}H_{26}O_{13,}$ m.p.: 263- 266 °C, optical activity: [α]/D-65 ± 8 C = 0.1 in methanol [35].

Antioxidant and anti-inflammatory activity

LPS is a key element of Gram-negative bacterial cell walls, which can induce a significant inflammatory response by stimulating the release of numerous inflammatory cytokines across various cell types [36]. In vitro, studies are valuable for examining cellular responses within a controlled environment where experimental conditions are consistently maintained. These studies are instrumental in elucidating the mechanisms behind the anti-inflammatory properties of herbal constituents. Various in vitro assays are employed to assess the anti-inflammatory effects of herbs [37].

Effect on reactive oxygen species (ROS)

ROS are the catalysts of "oxidative stress." In this context, antioxidants that can scavenge ROS play a crucial role in preventing this oxidative stress [38]. By measuring ROS in each sample and comparing to both LPS and negative controls, Fig. 3(i) shows that all samples had significantly lowered ROS compared to LPS-stimulated cells. The optimized extract was the most effective inhibitor of ROS than tiliroside. However, tiliroside was not significantly different compared to the negative control.

Effect on nitric oxide (NO) generation

NO is an essential signaling molecule in the progression of inflammation. In abnormal conditions, NO is a pivotal factor in managing inflammatory processes. As it regulates the functional activity of the inflammatory cells [39], Fig. 3(ii) demonstrates that tiliroside significantly reduced NO compared to the dexamethasone standard. Unfortunately, no significant variation was observed between the optimized extract and LPS-stimulated cells (Table 6). Although tiliroside demonstrated a higher percentage of NO inhibition than dexamethasone under the tested conditions, this observation should be interpreted cautiously. The assay was performed in triplicate, and while reproducibility was consistent across runs, further biological replicates and mechanistic studies are necessary to confirm this effect. These preliminary findings suggest that tiliroside may engage alternative or complementary anti-inflammatory pathways, potentially

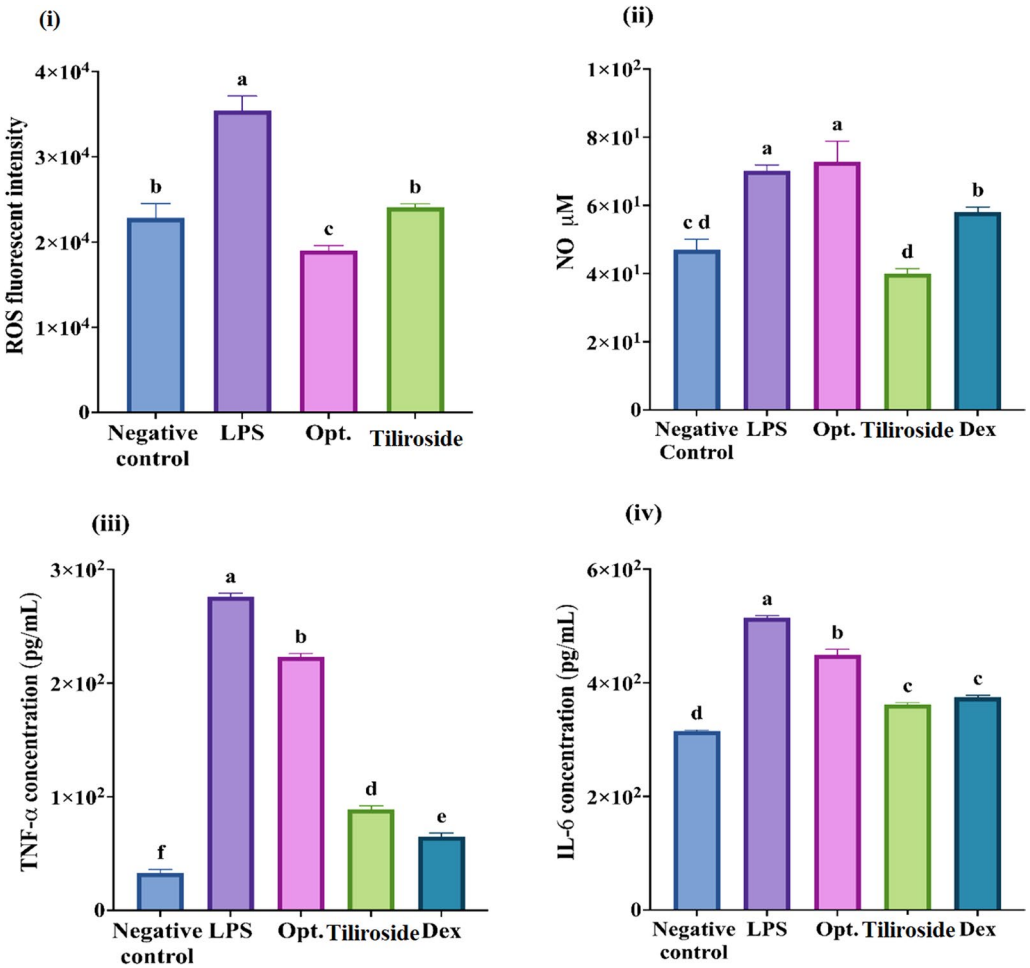


Fig. 3 Comparison of the effect of different studied groups on different performed bioassays, where **i** ROS fluorescence intensity, **ii** NO quantity, **iii** TNF-α concentration, **iv** IL-6 concentration. Negative control = untreated cell line, LPS = lipopolysaccharides, Opt. = optimized extract, Tiliroside = isolated compound, Dex = dexamethasone. Columns labeled with different letters indicate significant differences ($p < 0.05$), and columns with the same letters are not significantly different ($p > 0.05$)

offering a natural scaffold for therapeutic development. However, comparisons to synthetic glucocorticoids should be expanded using dose–response analyses and broader inflammatory models before firm conclusions can be drawn.

Effect on tumor necrosis factor-alpha (TNF-α)

TNF-α is a pleotropic cytokine that engages in orchestrating the inflammatory process. Therefore, the inhibition of TNF-α has been used as a potential target for the treatment of chronic inflammation [40, 41]. Figure 3 (iii) shows that tiliroside significantly reduced TNF-α than optimized extract, but on the other hand, dexamethasone had the best anti-inflammatory effect on TNF-α (Table 6).

Effect on Interleukin-6 (IL-6)

LPS is one of the several stimuli that generates the cytokine IL-6, which is also a major inducer of the acute inflammatory response. Furthermore, during chronic inflammation, IL-6 plays crucial functions in the immune response [41]. Figure 3 (iv) shows that all groups had significantly lower levels of IL-6 compared to the LPS-stimulated cells group (Table 6). Like dexamethasone, tiliroside decreased IL-6.

Post hoc test

Table 7 represents the results of one-way ANOVA for the distinct groups studied on different bioassays of *L. patersonii,* comparing the extracts to the negative control. Table 6 demonstrates the results of multiple comparisons conducted by post hoc test—Tukey's honestly significant difference (HSD) results. It is noteworthy that the

Table 6 The multiple comparison Post Hoc Test—Tukey's HSD results for the surviving extracts of *L. patersonii* comparing them to negative control

Studied group		Significance (*p*-value)			
		ROS	NO	TNF-*α*	IL-6
Group (I) versus group (5)					
Opt	Tiliroside	**0.002***	**0.000***	**0.000***	**0.000***
	Negative control	**0.012***	**0.000***	**0.000***	**0.000***
	LPS	**0.000***	0.892	**0.000***	**0.000***
	Dexamethasone	–	**0.001***	**0.000***	**0.000***
Tiliroside	Opt	**0.002***	**0.000***	**0.000***	**0.000***
	Negative control	0.660	0.118	**0.000***	**0.000***
	LPS	**0.000***	**0.000***	**0.000***	**0.000***
	Dexamethasone	–	**0.000***	**0.000***	0.063
Negative control	Opt	**0.012***	**0.000***	**0.000***	**0.000***
	Tiliroside	0.660	0.118	**0.000***	**0.000***
	LPS	**0.000***	**0.000***	**0.000***	**0.000***
	Dexamethasone	–	**0.008***	**0.000***	**0.000***
LPS	Opt	**0.000***	0.892	**0.000***	**0.000***
	Tiliroside	**0.000***	**0.000***	**0.000***	**0.000***
	Negative control	**0.000***	**0.000***	**0.000***	**0.000***
	Dexamethasone	–	**0.004***	**0.000***	**0.000***
Dexamethasone	Opt	–	**0.001***	**0.000***	**0.000***
	Tiliroside	–	**0.000***	**0.000***	0.063
	Negative control	–	**0.008***	**0.000***	**0.000***
	LPS	–	**0.004***	**0.000***	**0.000***

*The mean difference is significant at $P < 0.05$. Standard error for ROS = 905.52338. Standard error for NO = 2.46705. Standard error for TNF-*α* = 2.44949. Standard error for IL-6 = 4.03228. Group 1: Optimized extract (Opt.), Group 2: Tiliroside, Group 3: Negative control, Group 4: LPS, Group 5: Dexamethasone

Table 7 One-way ANOVA results for the distinct groups studied on different bioassays of *Lagunaria patersonii*

Bioassay	Studied groups	Sum of squares	DF	MS	F-value	Significance
ROS	Treatment (Between columns)	456,246,988	4	114,061,747	F (4, 10) = 92.7	$P < 0.001$*
	Residuals (Within columns)	12,299,589	10	1,229,959		
	Total	468,546,577	14			
NO	Treatment (Between columns)	2632	5	526	F (5, 12) = 57.7	$P < 0.001$
	Residuals (Within columns)	110	12	9.13		
	Total	2742	17			
TNF-α	Treatment (Between columns)	135,891	5	27,178	F (5, 12) = 3020	$P < 0.001$*
	Residuals (Within columns)	108	12	9		
	Total	135,999	17			
IL-6	Treatment (Between columns)	80,636	5	16,127	F (5, 12) = 661	$P < 0.001$
	Residuals (Within columns)	293	12	24.4		
	Total	80,928	17			

*The mean difference is significant at $P < 0.05$. Groups: Optimized extract (Opt.) and Tiliroside

optimized extract exerts a significant antioxidant effect (p-value < 0.05, Table 6). Conversely, tiliroside offers the most favorable anti-inflammatory effect with respect to the NO test, as it reduces the amount of NO significantly, even better than dexamethasone. However, it showed no significant difference (p-value > 0.05, Fig. 3) in inhibiting IL-6 compared to dexamethasone (Figs.3, 4, 5).

Tiliroside exhibited a broad and consistent inhibition of all inflammatory mediators, while the optimized extract was more potent against ROS (Table 8).

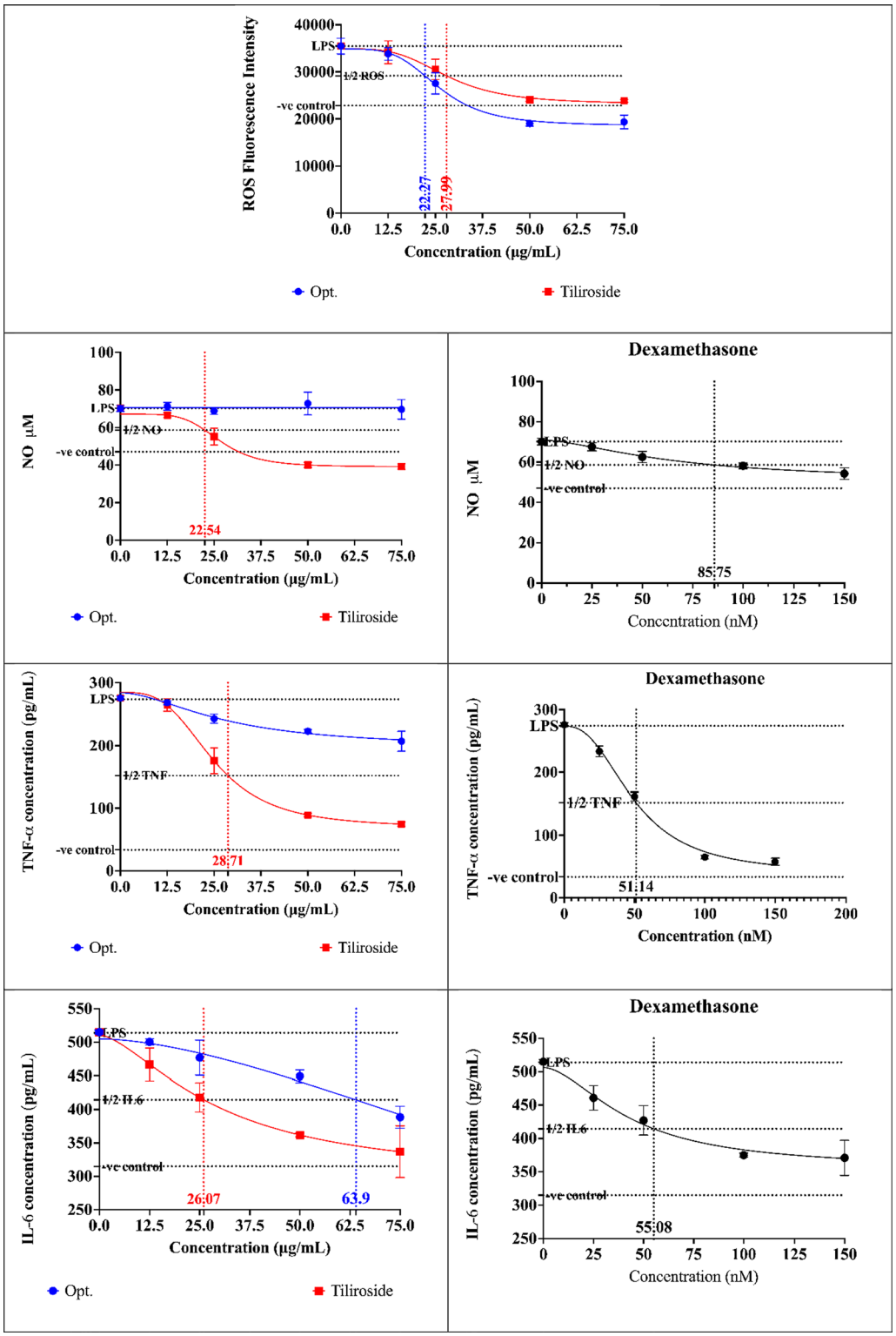


Fig. 4 Dose–response curves of ROS, NO, TNFα, and IL-6 in cells treated with tiliroside, optimized, and dexamethasone

Discussion

For the first time, an optimization study and UPLC-ESI-MS analysis for *L. patersonii* extract were performed. The method was developed to increase the yield of *L. patersonii* extract and investigate its antioxidant and anti-inflammatory activities by measuring inflammatory mediators (NO, TNF-α, IL-6). In agreement with [14], BBD method was efficient for establishing the optimization process. The established method significantly increased the yield of the plant extract, as well as the flavonoid content. Herein, optimization successfully increased the yield of tiliroside. Moreover, the experimental design has been verified, with high predictive power.

The optimization study revealed that extraction variables such as ethanol/water ratio, material/solvent ratio, and time do not act independently but interact significantly to influence both yield and extract composition. Specifically, while a higher material/solvent ratio enhanced yield, increasing ethanol content reduced it and this effect varied with extraction time. The significant negative impact of ethanol/water ratio on the 265/346 absorbance ratio highlights solvent polarity's role in modulating chromophore selectivity. These findings emphasize the practical importance of considering factor interactions to develop a more efficient, targeted extraction protocol, ensuring both high recovery and desired phytochemical profiles.

UPLC-ESI-MS was performed to track tiliroside concentration. The extracts of run two and run eleven exhibited the highest and lowest 265/346 absorbance ratio (0.729 and 0.512), respectively. Extract of run two exhibited the highest concentration of tiliroside and proved the concept of tracking the 265/346 absorbance ratio to maximize the tiliroside content in the extract. The optimized extract was conducted depending on maximizing both yield and the 265/346 absorbance ratio to maximize the yield of the tiliroside. This was confirmed by UPLC-ESI–MS, which showed the highest peak area that considered double the peak area of the highest run (run 2). After numerical optimization, the plant extracts with the highest yield and highest concentration of tiliroside showed a good association between the experimental and estimated values. It should be noted that the use of relative peak areas without absolute calibration may be subject to matrix effects and does not allow precise absolute quantification of tiliroside. Accordingly, the present findings should be interpreted as relative comparisons among samples. Future work will address this limitation by employing calibration with authentic standards to ensure higher accuracy.

A study by Abd-El-Aziz et al. [14] showed that the optimized ethanolic extract rich in quercetin, rutin, kaempferol, chlorogenic acid, and ρ-coumaric acid exhibited remarkable antioxidant and anti-inflammatory effects. Notably, the extract showed 80% free radical inhibition and potent anti-edematous effect comparable to indomethacin. These findings underscore the therapeutic potential of *L. hispidulus* and validate the efficiency of the applied extraction strategy for isolating biologically active phenolics.

Structural modification of kaempferol by acylation of glycosides with *p*-coumaric acid can significantly affect its absorption and bioactivity [42], which is consistent with the previous reports by Silva et al. [42], which highlighted the potential anti-inflammatory effect of some kaempferol glycosides through suppression of TNF-α and NO in LPS-induced inflammation. Similarly, Oppong et al. [43] documented that tiliroside has potential in vitro anti-inflammatory activity on some inflammatory targets such as COX-2 and phospholipase A2. It also showed the inhibition of NO production. Recent studies have elucidated multiple molecular pathways through which tiliroside exerts its anti-inflammatory effects. Notably, tiliroside has been shown to inhibit the NLRP3 inflammasome in macrophages by activating AMP-activated protein kinase (AMPK), which reduces mitochondrial ROS production and stabilizes mitochondrial membrane potential key steps in dampening inflammasome assembly and IL-1β release [44]. Additionally, tiliroside suppresses NF-κB and MAPK signaling pathways, leading to downregulation of pro-inflammatory mediators such as TNF-α, IL-6, iNOS, and COX-2 [45]. Molecular docking studies further support these findings, revealing strong binding affinities of tiliroside to key inflammatory targets including COX-2, iNOS, and JNK, suggesting direct molecular interactions that may underlie its bioactivity. These mechanisms collectively position tiliroside as

(See figure on next page.)

Fig. 5 The effect of tiliroside and optimized on the NFkB protein expression in the RAW 264.7 cell line. **i** The immunocytofluorescence photographs showing very high expression after LPS sensitization with subsequent decrease in the protein expression in both the tiliroside-treated cells and optimized-treated cells. **ii** One-way ANOVA analysis followed by Tukey's multiple comparisons test at a 95% confidence interval showing that the tiliroside significantly decreased the inflammatory NFkB protein expression than both the LPS-sensitized cells and the optimized extract. The optimized also inhibited the NFkB protein expression significantly than the LPS but still higher than the negative control cells. The data are represented as mean ± SD. The columns with the same letters are not significantly different. The scale bar is 20 µm

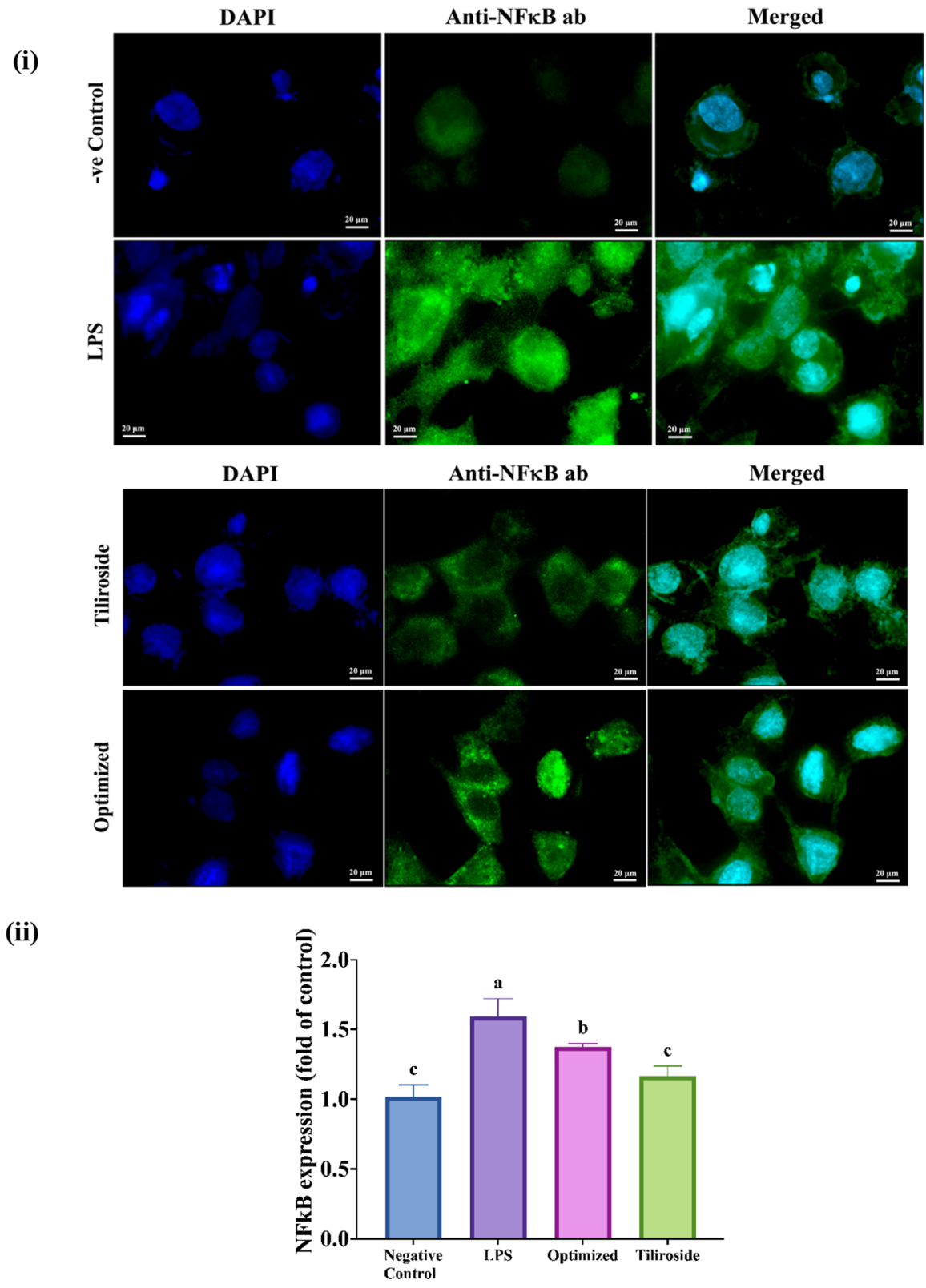


Fig. 5 (See legend on previous page.)

Table 8 The IC_{50} of tiliroside, optimized, and dexamethasone

IC_{50}	ROS	NO	TNFA	IL-6
Tiliroside (µg/mL)	27.99 ± 5.2	22.54 ± 6.3	28.71 ± 2.3	26.07 ± 9.6
Optimized (µg/mL)	22.27 ± 0.5	> 100	> 100	63.9 ± 10.9
Dexamethasone (nM)	–	85.75 ± 17.3	51.14 ± 4.2	55.08 ± 19.2

a promising multi-target anti-inflammatory agent with both upstream (signal transduction) and downstream (cytokine suppression) effects.

In line with these mechanistic insights, in vitro antioxidant and anti-inflammatory activities of the optimized extract and tiliroside were studied. Our immunofluorescence analysis confirmed that NF-κB expression was strongly upregulated following LPS stimulation but was significantly suppressed upon treatment with both tiliroside and the optimized extract (Fig. 5). Notably, tiliroside exerted greater inhibition than the optimized extract, indicating a more direct impact on NF-κB signaling. This is consistent with previous studies showing that NF-κB serves as a master regulator of macrophage-driven inflammation and that natural flavonoids can suppress NF-κB activation to reduce inflammatory mediator release [46, 47].

The dose–response assaysfurther highlighted differential inhibitory profiles of the two treatments (Fig. 4). Tiliroside consistently inhibited ROS, NO, TNF-α, and IL-6 with IC_{50} values in the range of 22–29 µg/mL, reflecting broad anti-inflammatory efficacy. Conversely, the optimized extract showed potent antioxidant activity (ROS $IC_{50} = 22.27$ µg/mL) but limited suppression of NO and TNF-α ($IC_{50} > 100$ µg/mL) and only moderate inhibition of IL-6. Compared to dexamethasone, tiliroside exhibited more potent inhibition of NO and comparable suppression of TNF-α and IL-6, though at higher concentrations. These findings suggest that while the optimized extract provides strong antioxidative protection, likely due to synergistic polyphenolic effects, tiliroside exerts more specific anti-inflammatory actions through inhibition of NF-κB and downstream cytokine signaling.

In summary, these results suggest that the optimized plant extract can be considered a natural source of antioxidants that may be essential to slow down the development of oxidative stress. This implies that the optimized extract may be effective in protecting cells from oxidative damage, and this activity may be attributed to the synergistic effect of the polyphenols in the optimized extract [48]. While tiliroside may be more effective at reducing inflammation and its associated symptoms and this could be explained by the fact that the other compounds in the optimized extract reduce the anti-inflammatory activity of tiliroside, so tiliroside is better on its own as anti-inflammatory and the optimized extract is better as antioxidant. These findings encourage further study to determine the exact mechanism of the antioxidant and the anti-inflammatory potential.

Conclusion

This study provides, for the first time, a validated method for the optimization of *L. patersonii* and investigation of its antioxidant and anti-inflammatory activities. The BBD of the plant extraction employing RSM was a valuable way to investigate the impact of the studied factors and their interactions on the extraction yield and the tiliroside content in the plant extract. UPLC-ESI–MS was successfully applied to track tiliroside concentration and proved the success of the economically employed wavelength absorbance approach, which mirrors the abundance of tiliroside, to increase its amount. In vitro antioxidants and anti-inflammatory activities revealed that the optimized plant extract exhibited high antioxidant activity, while tiliroside, showed high anti-inflammatory activity targeting NO, TNF-α, and IL-6. *L. patersonii* was proven to be a reliable source of natural antioxidants and anti-inflammatories. Further research is recommended to identify the other compounds contributing to the antioxidant activities of the optimized extract. On the other hand, the proposed wavelength absorbance approach simple, cost-effective, and adaptable can be extended to other phytoconstituents exhibiting dual absorbance maxima, such as flavonoid glycosides or phenolic acids. Future studies may apply this method to other medicinal plant species to streamline compound quantification and correlate spectrophotometric profiles with biological activities.

Abbreviations

DOE	Design of experiment
BBD	Box–Behnken design
ANOVA	Analysis of variance
ROS	Reactive oxygen species
TNF-α	Tumor necrosis factor-alpha
ELISA	Enzyme-linked immunosorbent assay
NO	Nitric oxide
NSAIDs	Non-steroidal anti-inflammatory drugs
COX-2	Cyclooxygenase-2
DMEM	Dulbecco's modified Eagle medium
LPS	Lipopolysaccharides
IL-6	Interleukin-6
ESI- MS	Electron spray ionization Mass spectrometry
UPLC	Ultra-performance liquid chromatography
UV	Ultraviolet

SPSS Statistical Package for Social Sciences
HSD Honestly significant difference

Supplementary Information

The online version contains supplementary material available at https://doi.org/10.1186/s43094-025-00913-4.

Additional file1 (DOCX 571 KB)

Author contributions

Mayar M. Eladl: writing original draft, visualization, methods, investigation, conceptualization. Ahmed A. El-Ashmawy: writing original draft, reviewing, and editing, visualization, methods, investigation, conceptualization. Mahmoud T. Abo-Elfadl: reviewing, and editing, visualization, methods, investigation. Nabaweya M. El-Fiky: reviewing, and editing, visualization, methods, investigation, conceptualization. Nabil M. Selim: reviewing, and editing, visualization, methods, investigation, conceptualization. Amira K. Elmotayam: reviewing, and editing, visualization, methods, investigation, conceptualization.

Availability of data and materials

Data will be made available upon request.

Declarations

Ethics approval and consent to participate

Not applicable.

Consent for publication

Not applicable.

Competing interests

The authors declare no competing interests.

Plant authentication

Fresh leaves of L. patersonii (Andrews) G. Don. were collected from the private garden ''El-Abd Botanical Garden '' (Cairo Alex. Desert Road, Egypt) in January 2022. The collection of plant was established after the required permission from Agricultural Research Center, Giza, Egypt. The plant was authenticated by Mrs. Therese Labib, a specializing consultant in botanical gardens and plant taxonomy. A sample voucher numbered 27.02.2022I, has been preserved in the herbarium of the Department of Pharmacognosy, Faculty of Pharmacy, Cairo University.

Author details

[1]Department of Pharmacognosy, Faculty of Pharmacy, Cairo University, Kasr El Aini St., Cairo 11562, Egypt. [2]Medicinal and Pharmaceutical Chemistry Department, Pharmaceutical and Drug Industries Research Institute, National Research Centre, 33 EL Bohouth St. (former EL Tahrir St.), P.O. 12622 Dokki, Giza, Egypt. [3]Cancer Biology and Genetics Laboratory, Centre of Excellence for Advanced Sciences, National Research Centre, Dokki, Giza 12622, Egypt. [4]Biochemistry Department, Biotechnology Research Institute, National Research Centre, Dokki, Giza, Egypt.

Received: 27 March 2025 Accepted: 11 November 2025
Published online: 24 November 2025

References

1. Christenhusz MJ, Byng JW (2016) The number of known plants species in the world and its annual increase. Phytotaxa 261(3):201–217
2. Bayer C, Kubitzki K (2006) Malvaceae. Springer
3. Shamso E, Khattab A (2016) Phenetic relationship between Malvaceae ss and its related families. Taeckholmia 36(1):115–135. https://doi.org/10.21608/taec.2016.11956
4. Kuppusamy S, Thavamani P, Megharaj M, Nirola R, Lee YB, Naidu R (2016) Assessment of antioxidant activity, minerals, phenols, and flavonoid contents of common plant/tree waste extracts. Ind Crops Prod 83:630–634. https://doi.org/10.1016/j.indcrop.2015.12.060
5. ElALFY TS, EL Tanbouly ND, El-Tantawy ME, Saleh AY (1994) Insecticide of plant origin part 1. Bull Fac Pharm Cairo Univ 32(3):423–426
6. Ruban P, Gajalakshmi K (2012) In vitro antibacterial activity of *Hibiscus rosa–sinensis* flower extract against human pathogens. Asian Pac J Trop Biomed 2(5):399–403
7. Nirmal CR et al (2020) Anti-tuberculosis activity of bio-active compounds from *Lantana camara* L., *Euphorbia hirta* L., *Mukia maderaspatana* (L.) M. Roem, and *Abutilon indicum* (L.). Eur J Integr Med 35:101105
8. Vadivel V (2016) Distribution of flavonoids among Malvaceae family members–A review. Int J Green Pharm 10(1)
9. Oliveira MS et al (2024) Chemical constituents, antioxidant and antimicrobial activities of Pavonia glazioviana Gurke (Malvaceae). Quim Nova 48(1):e20250011
10. Malheiros J, Simões DM, Antunes PE, Figueirinha A, Cotrim MD, Fonseca DA (2022) Vascular effects of polyphenols from *Agrimonia eupatoria* L. and role of isoquercitrin in its vasorelaxant potential in human arteries. Pharmaceuticals 15(5):638
11. Hemdan SS, Al Jebaly AM, Ali FK (2019) Importance of isosbestic point in spectroscopy: a review. J Sci Hum Stud 62:1–21
12. McNaught AD, Wilkinson A (1997) Compendium of chemical terminology. Blackwell Science, Oxford
13. Verma G, Mishra M (2018) Development and optimization of UV-Vis spectroscopy review. World J Pharm Res 7(11):1170–1180
14. Abd-El-Aziz NM, Hifnawy MS, El-Ashmawy AA, Lotfy RA, Younis IY (2022) Application of Box-Behnken design for optimization of phenolics extraction from *Leontodon hispidulus* in relation to its antioxidant, anti-inflammatory, and cytotoxic activities. Sci Rep 12(1):8829
15. Elsayed EW, El-Ashmawy AA, Mursi NM, Emara LH (2019) Optimization of gliclazide-loaded alginate-gelatin beads employing central composite design. Drug Dev Ind Pharm 45(12):1959–1972
16. Toyota H, Asai T, Oku N (2017) Process optimization by use of design of experiments: application for liposomalization of FK506. Eur J Pharm Sci 102:196–202
17. Wafa SSAE et al (2023) Optimization of oil yield of Pelargonium graveolens L'Hér using Box-Behnken design in relation to its antimicrobial activity and in silico study. Sci Rep 13(1):19887
18. Abu-Dahab R, Afifi F (2007) Antiproliferative activity of selected medicinal plants of Jordan against a breast adenocarcinoma cell line (MCF7). Scientia Pharm 75(3):121–146
19. Hwang E-S, Do Thi N (2014) Effects of extraction and processing methods on antioxidant compound contents and radical scavenging activities of laver (*Porphyra tenera*). Prev Nutr Food Sci 19(1):40
20. Ferreira SC et al (2007) Box-Behnken design: An alternative for the optimization of analytical methods. Anal Chim Acta 597(2):179–186
21. Ahmad A, Alkharfy KM, Wani TA, Raish M (2015) Application of Box–Behnken design for ultrasonic-assisted extraction of polysaccharides from Paeonia emodi. Int J Biol Macromol 72:990–997
22. Ranneh Y, Ali F, Akim AM, Hamid HA, Khazaai H, Fadel A (2017) Crosstalk between reactive oxygen species and pro-inflammatory markers in developing various chronic diseases: a review. Appl Biol Chem 60:327–338
23. Zhao F, Wang L, Liu K (2009) In vitro anti-inflammatory effects of arctigenin, a lignan from *Arctium lappa* L., through inhibition of the iNOS pathway. J Ethnopharmacol 122(3):457–462
24. Bindu S, Mazumder S, Bandyopadhyay U (2020) Non-steroidal anti-inflammatory drugs (NSAIDs) and organ damage: a current perspective. Biochem Pharmacol 180:114147
25. Das G et al (2021) Systematics, phytochemistry, biological activities, and health-promoting effects of the plants from the subfamily Bombacoideae (family Malvaceae). Plants 10(4):651
26. Kumar SP, Singh SS, Singh NP, Mayur P (2011) In vitro antioxidant activity of *Gossypium herbaceum* Linn. Int Res J Pharm 2(7):166–170
27. Jaroennoni P, Sithisarn P, Rojsanga P (2017) Optimization of antioxidant extraction from *Persicaria barbata* leaves using response surface methodology (RSM). Extraction 1:0
28. Che Sulaiman IS, Basri M, Fard Masoumi HR, Chee WJ, Ashari SE, Ismail M (2017) Effects of temperature, time, and solvent ratio on the extraction of phenolic compounds and the anti-radical activity of *Clinacanthus nutans* Lindau leaves by response surface methodology. Chem Cent J 11(1):1–11

29. Yoo G, Lee IK, Park S, Kim N, Park JH, Kim SH (2018) Optimization of extraction conditions for phenolic acids from the leaves of *Melissa officinalis* L. using response surface methodology. Pharmacogn Mag 14(54):155
30. Chung C-Y, Duchen MR (2022) A plate reader-based measurement of the cellular ROS production using dihydroethidium and MitoSOX. Mitochondria: Methods and Protocols. Springer, pp 333–337
31. Ranaweera SS, Dissanayake CY, Natraj P, Lee YJ, Han C-H (2020) Anti-inflammatory effect of sulforaphane on LPS-stimulated RAW 264.7 cells and ob/ob mice. J Vet Sci 21(6)
32. Laksmitawati DR et al (2017) Anti-inflammatory effects of Anredera cordifolia and Piper crocatum extracts on lipopolysaccharide-stimulated macrophage cell line. Bangladesh J Pharmacol 12(1):35–40
33. Vijayalakshmi P, Devi VK, Narendra C, Srinagesh S (2008) Development of extended zero-order release gliclazide tablets by central composite design. Drug Dev Ind Pharm 34(1):33–45
34. Mundada PK, Sawant KK, Mundada VP (2017) Formulation and optimization of controlled release powder for reconstitution for metoprolol succinate multi-unit particulate formulation using risk-based QbD approach. J Drug Deliv Sci Technol 41:462–474
35. Gudej J (2003) Kaempferol and quercetin glycosides from *Rubus idaeus* L. leaves. Acta Pol Pharm 60(4):313–316
36. Ngkelo A, Meja K, Yeadon M, Adcock I, Kirkham PA (2012) LPS-induced inflammatory responses in human peripheral blood mononuclear cells is mediated through NOX4 and G *i* α dependent PI-3kinase signalling. J Inflamm 9:1–7
37. Sarveswaran R, Jayasuriya W, Suresh T (2017) In vitro assays to investigate the anti-inflammatory activity of herbal extracts: a review. World J Pharm Res
38. Zhang C, Wang X, Du J, Gu Z, Zhao Y (2021) Reactive oxygen species-regulating strategies based on nanomaterials for disease treatment. Adv Sci 8(3):2002797
39. Sharma J, Al-Omran A, Parvathy S (2007) Role of nitric oxide in inflammatory diseases. Inflammopharmacology 15:252–259
40. Vassalli P (1992) The pathophysiology of tumor necrosis factors. Annu Rev Immunol 10(1):411–452
41. Sittisart P, Chitsomboon B, Kaminski NE (2016) Pseuderanthemum palatiferum leaf extract inhibits the proinflammatory cytokines, TNF-α and IL-6 expression in LPS-activated macrophages. Food Chem Toxicol 97:11–22
42. dos Silva Santos J, Goncalves Cirino JP, de Oliveira Carvalho P, Ortega MM (2021) The pharmacological action of kaempferol in central nervous system diseases: a review. Front Pharmacol 11:565700
43. Oppong MB et al (2024) In-vitro and in-vivo anti-inflammatory properties of extracts and isolates of Pangdahai. Phytomed Plus. 4(2):100533
44. Zhong et al (2023) Tiliroside attenuates NLRP3 inflammasome activation in macrophages and protects against acute lung injury in mice. Molecules 28(22):7527
45. Kaur et al (2024) Multifaceted Role of Tiliroside in Inflammatory Pathways: Mechanisms and Prospects. Recent Adv Inflamm Aller Drug Discov
46. Liu YY et al (2013) Suppressing NF-κB and NKRF pathways by induced pluripotent stem cell therapy in mice with ventilator-induced lung injury. PLoS ONE 8(6):e66760
47. Al-Khayri JM et al (2022) Flavonoids as potential anti-inflammatory molecules: a review. Molecules. https://doi.org/10.3390/molecules27092901
48. Joshi T, Deepa P, Sharma PK (2022) Effect of different proportions of phenolics on antioxidant potential: pointers for bioactive synergy/antagonism in foods and nutraceuticals. Proc Natl Acad Sci India Sect B Biol Sci 92(4):939–946

Publisher's Note

Springer Nature remains neutral with regard to jurisdictional claims in published maps and institutional affiliations.